②LEVEL Ⅲ   AD-E200519

ADA086815

INTERACTION BETWEEN A PARALLEL-PLATE EMP SIMULATOR AND A CYLINDRICAL TEST OBJECT

J. Lam

Dikewood Industries, Inc.
1009 Bradbury Drive, SE
Albuquerque, NM 87106

May 1980

Final Report

Approved for public release; distribution unlimited.

DTIC
S ELECTE D
JUL 17 1980

B

AIR FORCE WEAPONS LABORATORY
Air Force Systems Command
Kirtland Air Force Base, NM 87117

80 6 10 007

This final report was prepared by Dikewood Industries, Inc., Albuquerque, New Mexico, under Contract F29601-78-C-0045, Job Order 37630274 with the Air Force Weapons Laboratory, Kirtland Air Force Base, New Mexico. Captain Howard G. Hudson (NTYE) was the Laboratory Project Officer-in-Charge.

This report has been reviewed by the Public Affairs Office and is releasable to the National Technical Information Service (NTIS). At NTIS, it will be available to the general public, including foreign nations.

This technical report has been reviewed and is approved for publication.

HOWARD G. HUDSON
Captain, USAF
Project Officer

J. PHILIP CASTILLO, PhD
Chief, Electromagnetics Branch

FOR THE DIRECTOR

THOMAS W. CIAMBRONE
Colonel, USAF
Chief, Applied Physics Division

REPORT DOCUMENTATION PAGE		READ INSTRUCTIONS BEFORE COMPLETING FORM
1. REPORT NUMBER AFWL-TR-79-138	2. GOVT ACCESSION NO. AD-A086 845	3. RECIPIENT'S CATALOG NUMBER
4. TITLE (and Subtitle) INTERACTION BETWEEN A PARALLEL-PLATE EMP SIMULATOR AND A CYLINDRICAL TEST OBJECT		5. TYPE OF REPORT & PERIOD COVERED Final Report
		6. PERFORMING ORG. REPORT NUMBER DC-FR-1299-3
7. AUTHOR(s) J. Lam		8. CONTRACT OR GRANT NUMBER(s) F29601-78-C-0045
9. PERFORMING ORGANIZATION NAME AND ADDRESS Dikewood Industries, Inc. 1009 Bradbury Drive, S.E. Albuquerque, NM 87106		10. PROGRAM ELEMENT, PROJECT, TASK AREA & WORK UNIT NUMBERS 64711F/37630274
11. CONTROLLING OFFICE NAME AND ADDRESS Air Force Weapons Laboratory (NTYE) Kirtland Air Force Base, NM 87117		12. REPORT DATE May 1980
		13. NUMBER OF PAGES 38
14. MONITORING AGENCY NAME & ADDRESS(if different from Controlling Office)		15. SECURITY CLASS. (of this report) Unclassified
		15a. DECLASSIFICATION/DOWNGRADING SCHEDULE

16. DISTRIBUTION STATEMENT (of this Report)

Approved for public release; distribution unlimited.

17. DISTRIBUTION STATEMENT (of the abstract entered in Block 20, if different from Report)

18. SUPPLEMENTARY NOTES

19. KEY WORDS (Continue on reverse side if necessary and identify by block number)

Electromagnetic Pulse (EMP)　　　　　　　Singularity Expansion Method
Parallel-Plate EMP Simulator
Test-Object/Simulator Interaction
Natural Frequencies

20. ABSTRACT (Continue on reverse side if necessary and identify by block number)

The interaction between a bounded-wave EMP simulator and a test object is studied with a geometrical model. The model consists of a finite, open-ended cylinder inside a parallel-plate waveguide. The interaction problem is formulated exactly by means of an integrodifferential equation, which is subsequently reduced to a matrix equation. An approximate analytical solution of the matrix equation is obtained. The singularities of the solution in the complex-frequency plane are investigated. The effects of the

DD $_{1\ JAN\ 73}^{FORM}$ 1473

20. ABSTRACT

simulator/test-object interaction on the pole singularities are numerically evaluated.

CONTENTS

ACCESSION for

NTIS   White Section ☑
DDC   Buff Section ☐
UNANNOUNCED   ☐
JUSTIFICATION _____

BY ___
DISTRIBUTION/AVAILABILITY CODES

Dist.   AVAIL. and/or SPECIAL

A

1

ILLUSTRATIONS

TABLES

SECTION I

INTRODUCTION

Bounded-wave electromagnetic-pulse (EMP) simulators provide one means to generate simulated EMP's for testing the EMP responses of aircraft and missiles on the system level (ref. 1). A simulator can be designed to launch an electromagnetic pulse into the simulator volume which closely approximates the actual nuclear EMP. This ability, however, does not imply that the actual interaction between the nuclear EMP and the test object is also thereby automatically closely simulated. In the simulator there exists an additional interaction between the simulator structure and the test object which is absent in the actual EMP encounter in free space. This interaction adversely affects the quality of the simulation. In order to interpret and utilize correctly the simulator test data, it is necessary to estimate and make allowance for this simulator/test-object interaction.

This report presents an analytical study of the simulator/test-object interaction. It employs an idealized model with simplified geometries to keep the mathematics manageable. The bounded-wave EMP simulator is modeled by a pair of parallel, perfectly conducting, flat plates of infinite extent, as depicted in figure 1. Such a structure is an electromagnetic waveguide. Let the spacing between the two plates be denoted by h. A rectangular coordinate system can be set up such that the lower plate is at $z = 0$ and the upper plate at $z = h$. The test object is taken to be a hollow cylinder or tube of cross-sectional radius a and length L. It is considered to be perfectly conducting and of infinitesimal thickness. The axis of the tube is oriented perpendicular to the two plates, and can be taken to coincide with the z-axis. The length L is then of necessity less than h. Let the lower end of the tube be at a height b above the lower plate.

The tube is a sufficiently simple model of a missile or aircraft structure, while the infinite plates constitute an idealization of the parallel-plate section of a bounded-wave simulator. By choosing this idealized model, it is possible to perform a rigorous and exact formulation of the simulator/test-object interaction problem which is at the same time not too complicated for an analytical solution.
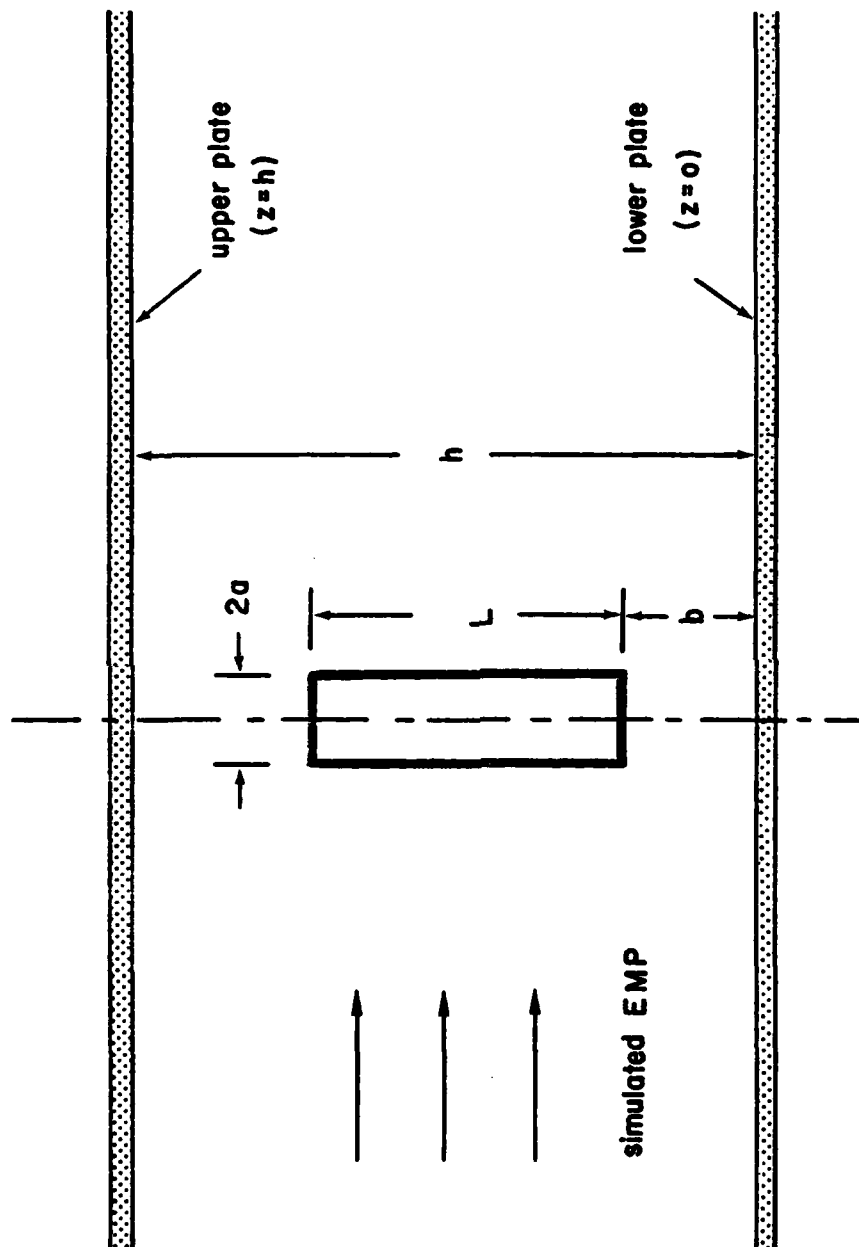
3

Figure 1. Geometry of the Interaction Between a Parallel-Plate Simulator and a Cylindrical Test Object

4

SECTION II

ELECTROMAGNETIC POTENTIALS

The specific goal of this analysis is to calculate the electric current induced on the cylinder when the parallel-plate waveguide is excited by an electromagnetic wave. This electromagnetic wave can, for example, be a simulated EMP in the form of the transverse-electromagnetic (TEM) mode of the waveguide. The effect of the simulator/test-object interaction is estimated by comparing this induced current with its corresponding value when the cylinder is excited in free space in the absence of the simulator.

The current induced on the cylinder by an incident electromagnetic wave in the parallel-plate waveguide can be evaluated by solving an integro-differential equation. The derivation of this equation requires a considerable amount of calculation. One first introduces the electromagnetic scalar and vector potentials V and $\underline{A}$ for the electromagnetic fields $\underline{E}^{sc}$ and $\underline{B}^{sc}$ scattered off the cylinder and the plates, such that

$$\underline{E}^{sc}(\underline{r},t) = - \nabla V(\underline{r},t) - \frac{\partial}{\partial t}\underline{A}(\underline{r},t) \ , \quad \underline{B}^{sc}(\underline{r},t) = \nabla \times \underline{A}(\underline{r},t) \qquad (1)$$

In the Lorentz gauge these potentials are related by the Lorentz condition:

$$\nabla \cdot \underline{A}(\underline{r},t) + \frac{1}{c^2}\frac{\partial}{\partial t} V(\underline{r},t) = 0 \qquad (2)$$

and individually satisfy the wave equation:

$$\left(\nabla^2 - \frac{1}{c^2}\frac{\partial^2}{\partial t^2}\right)V(\underline{r},t) = 0 \ , \quad \left(\nabla^2 - \frac{1}{c^2}\frac{\partial^2}{\partial t^2}\right)\underline{A}(\underline{r},t) = 0 \qquad (3)$$

At $z = 0$ and h, on the surfaces of the two parallel plates, the tangential components of $\underline{E}^{sc}$ and the normal component of $\underline{B}^{sc}$ must vanish. By writing out equations (1) and (2) in rectangular component form, one can easily convince oneself that these boundary conditions on the fields imply the following boundary conditions on the potentials:

5

$$V(\underline{r},t) = A_x(\underline{r},t) = A_y(\underline{r},t) = 0$$

(4)

$$\frac{\partial}{\partial z} A_z(\underline{r},t) = 0$$

for $z = 0$ and h . Thus the scalar potential and the tangential components of the vector potential satisfy the homogeneous Dirichlet boundary condition on the plates, while the normal component of the vector potential satisfies the homogeneous Neumann boundary condition.

It will be convenient to go over from the time variable t to a complex frequency variable s by introducing the Laplace transforms of all time-dependent quantities. For example, the Laplace transform of the scalar potential is

$$V(\underline{r},s) = \int_{-\infty}^{\infty} dt\ e^{-st} V(\underline{r},t)$$

(5)

Under this transformation equations (3) become

$$(\nabla^2 - \gamma^2) V(\underline{r},s) = 0 \ , \quad (\nabla^2 - \gamma^2)\underline{A}(\underline{r},s) = 0$$

(6)

where

$$\gamma = \frac{s}{c}$$

(7)

Their solutions can be represented as definite integrals over the surface of the cylinder:

$$V(\underline{r},s) = \frac{1}{\varepsilon_o} \int G_D(\underline{r},\underline{r}',s)\sigma(\underline{r}',s)dS'$$

$$A_x(\underline{r},s) = \mu_o \int G_D(\underline{r},\underline{r}',s)K_x(\underline{r}',s)dS'$$

$$A_y(\underline{r},s) = \mu_o \int G_D(\underline{r},\underline{r}',s)K_y(\underline{r}',s)dS'$$

$$A_z(\underline{r},s) = \mu_o \int G_N(\underline{r},\underline{r}',s)K_z(\underline{r}',s)dS'$$

(8)

6

In these expressions, σ and $\underline{K}$ are the surface charge and current densities induced on the cylinder by the incident wave; G_D and G_N are the Green's functions for the Dirichlet and Neumann boundary-value problems of the parallel-plate waveguide; and the field position vector $\underline{r} = (x,y,z)$ stands for a point in space while the source position vector $\underline{r}' = (x',y',z')$ stands for a point on the surface of the cylinder.

The Green's functions G_D and G_N are solutions of the nonhomogeneous Helmholtz equation:

$$(\nabla^2 - \gamma^2)G_D(\underline{r},\underline{r}',s) = - \delta^3(\underline{r} - \underline{r}')$$

$$(\nabla^2 - \gamma^2)G_N(\underline{r},\underline{r}',s) = - \delta^3(\underline{r} - \underline{r}')$$

$$(9)$$

They satisfy, respectively, the homogeneous Dirichlet boundary condition $G_D = 0$ and the homogeneous Neumann boundary condition $\partial G_N/\partial z = 0$ on the plates $z = 0$ and h . In addition they both satisfy the outgoing-wave condition at infinity. Using standard Green's function techniques, one finds that

$$G_D(\underline{r},\underline{r}',s) = \sum_{n=1}^{\infty} U_n(x,y,x',y',s)\sin p_n z \sin p_n z'$$

$$(10)$$

$$G_N(\underline{r},\underline{r}',s) = \sum_{n=0}^{\infty} U_n(x,y,x',y',s)\cos p_n z \cos p_n z'$$

with

$$p_n = \frac{n\pi}{h} \tag{11}$$

and

$$U_n(x,y,x',y',s) = \frac{1}{\pi h \epsilon_n} K_0\left(\sqrt{\gamma^2 + p_n^2} \, R\right) \tag{12}$$

Here K_0 is a modified Bessel function,

$$R = \sqrt{(x-x')^2 + (y-y')^2} \tag{13}$$

and ϵ_n is defined by:

$$\epsilon_n = \begin{cases} 2 & n = 0 \\ 1 & n = 1,2,3,\ldots \end{cases} \tag{14}$$

7

Furthermore, to satisfy the outgoing-wave condition, the branch of the square root in equation (12) is to be chosen to make

$$\sqrt{\gamma^2 + p_n^2} \rightarrow \gamma \qquad (15)$$

as $\gamma \rightarrow \infty$.

SECTION III

DERIVATION OF INTEGRODIFFERENTIAL EQUATION

The surface charge density σ can be eliminated from the calculation by using the continuity equation:

$$s\sigma(\underline{r},s) + \nabla \cdot \underline{K}(\underline{r},s) = 0 \tag{16}$$

The independent unknown quantities of the problem are then the two components of the surface current density $\underline{K}$. One can set up two integrodifferential equations for $\underline{K}$ by applying the boundary conditions on the tangential components of the total electric field on the surface of the cylinder. In a standard cylindrical coordinate system (ρ,φ,z) with polar axis coinciding with the axis of the cylinder, these boundary conditions are

$$E_z^{inc}(\underline{r},s) + E_z^{sc}(\underline{r},s) = 0 \ , \qquad E_\varphi^{inc}(\underline{r},s) + E_\varphi^{sc}(\underline{r},s) = 0 \tag{17}$$

for $\underline{r}$ on the cylinder.

The two integrodifferential equations so derived are generally coupled. However, for the specific geometry of this problem, it is possible to obtain from them a single closed integrodifferential equation for the total axial current I defined as

$$I(z,s) = a \int_0^{2\pi} d\varphi \ K_z(\varphi,z,s) \tag{18}$$

The total axial current by itself is often sufficient to characterize the excitation of a thin cylinder at low frequencies, since in this limit the circumferential current is small by comparison.

To derive the integrodifferential equation for the total axial current I , one writes down the first of the boundary conditions (17) in terms of the potentials:

$$\frac{\partial}{\partial z} V(\underline{r},s) + s A_z(\underline{r},s) = E_z^{inc}(\underline{r},s) \tag{19}$$

9

Substituting the integral representations (8) of the potentials into equation (19) and eliminating the surface charge density σ by use of equation (16), one obtains

$$\frac{\partial}{\partial z} \int G_D(\underline{r},\underline{r}',s) \left[\frac{1}{a} \frac{\partial}{\partial \varphi'} K_\varphi(\underline{r}',s) + \frac{\partial}{\partial z'} K_z(\underline{r}',s) \right] dS'$$

$$- \gamma^2 \int G_N(\underline{r},\underline{r}',s) K_z(\underline{r}',s) dS' = - s\epsilon_o E_z^{inc}(\underline{r},s)$$

(20)

This equation holds for $b < z,z' < L+b$, with

$$\underline{r} = (a,\varphi,z) , \qquad \underline{r}' = (a,\varphi',z')$$

(21)

and

$$\int dS' = a \int_0^{2\pi} d\varphi' \int_b^{L+b} dz'$$

(22)

It is to be especially noted that, in the cylindrical coordinates, the two Green's functions G_D and G_N depend on the two azimuthal angles φ and φ' only through the cosine of their difference $\varphi - \varphi'$, so that

$$G_D(\underline{r},\underline{r}',s) = G_D(\cos(\varphi-\varphi'), z,z',s)$$

(23)

$$G_N(\underline{r},\underline{r}',s) = G_N(\cos(\varphi-\varphi'), z,z',s)$$

This property is of vital importance in the following derivation of the integro-differential equation for I .

If one integrates both sides of equation (20) over φ from 0 to 2π , two important events take place. First, the φ'-dependence of the Green's functions drops out:

$$\int_0^{2\pi} d\varphi \, G_D(\cos(\varphi-\varphi'), z,z',s) = \int_0^{2\pi} d\psi \, G_D(\cos \psi, z,z',s)$$

$$= 2\pi \, \Gamma_D(z,z',s)$$

$$\int_0^{2\pi} d\varphi \, G_N \, (\cos(\varphi - \varphi'), \, z, z', s) = \int_0^{2\pi} d\psi \, G_N(\cos \psi, \, z, z', s)$$

$$= 2\pi \, \Gamma_N(z, z', s) \tag{24}$$

Therefore the subsequent φ'-integration in equation (20) is carried out solely on the surface current density components K_φ and K_z. Second, the term in K_φ vanishes after the φ'-integration because

$$\int_0^{2\pi} d\varphi' \, \frac{\partial}{\partial \varphi'} \, K_\varphi(\underline{r}', s) = K_\varphi(\underline{r}', s) \Big|_{\varphi' = 0}^{\varphi' = 2\pi} = 0 \tag{25}$$

On the other hand the φ'-integration of K_z yields directly the total axial current I, as defined in equation (18). Gathering together all these results, one obtains the following nonhomogeneous integro-differential equation for I :

$$\frac{\partial}{\partial z} \int_b^{L+b} dz' \Gamma_D(z, z', s) \frac{\partial}{\partial z'} I(z', s)$$

$$\tag{26}$$

$$- \gamma^2 \int_b^{L+b} dz' \Gamma_N(z, z', s) I(z', s) = - s \varepsilon_0 \overline{E}_z^{inc}(z, s)$$

where

$$\overline{E}_z^{inc}(z, s) = \frac{1}{2\pi} \int_0^{2\pi} d\varphi \, E_z^{inc}(a, \varphi, z, s) \tag{27}$$

That is, $\overline{E}_z^{inc}$ is the average value of the z-component of the incident electric field around the circumference of the cylinder at a fixed value of z.

One should emphasize that equation (26) is an exact equation. No approximation has been invoked in its derivation. This remarkable, rigorous result is actually made possible through the judicious choice of the geometry of the model. If a different geometry were chosen, it is doubtful that a closed equation for I similar to equation (26) could be derived without the help of assumptions and approximations.

11

The two functions Γ_D and Γ_N in equation (26) can be evaluated explicitly in closed form. Substituting equation (10) into equation (24), one obtains

$$\Gamma_D(z,z',s) = \sum_{n=1}^{\infty} W_n(s)\sin p_n z \sin p_n z'$$

$$\Gamma_N(z,z',s) = \sum_{n=0}^{\infty} W_n(s)\cos p_n z \cos p_n z' \tag{28}$$

where

$$W_n(s) = \frac{1}{2\pi}\int_0^{2\pi} d\psi \; \frac{1}{\pi h \epsilon_n} K_0\left(2a\sqrt{\gamma^2 + p_n^2} \sin \frac{\psi}{2}\right)$$

$$= \frac{1}{\pi h \epsilon_n} I_0\left(\sqrt{\gamma^2 + p_n^2}\; a\right) K_0\left(\sqrt{\gamma^2 + p_n^2}\; a\right) \tag{29}$$

Use has been made of the addition theorem for the cylindrical functions (ref. 2) in evaluating the integral in equation (29).

SECTION IV

REDUCTION TO MATRIX EQUATION

Equation (26) is a second-order integrodifferential equation. It
therefore requires the specification of two boundary conditions in the
coordinate z for the unique determination of the total axial current I.
These boundary conditions can be taken as the two end conditions.

$$I(z,s) = 0 \quad \text{for} \quad z = b \text{ and } L+b \quad (30)$$

However, it is often inconvenient to treat the problem in hand directly as a
two-point boundary-value problem for equation (26). For the purposes of
analytical approximation or numerical solution, much advantage can be gained
by combining equation (26) and the boundary conditions (30) and reducing them
to a single matrix equation.

The transition to a matrix equation is achieved by going over to a
discrete system of description. To this end one introduces a complete set
of mutually orthogonal functions over the interval $b < z < L+b$ which
vanish at the two end points $z = b$ and $L+b$. This set consists of the
sine functions $\sin k_m(z-b)$ with

$$k_m = \frac{m\pi}{L} \qquad m = 1,2,3,\ldots \quad (31)$$

These functions can be considered as the orthogonal basis vectors of an infinite-
dimensional vector space. The current I, satisfying the boundary conditions
(30), can be expanded in terms of these basis vectors:

$$I(z,s) = \sum_{m=1}^{\infty} C_m(s)\sin k_m(z-b) \quad (32)$$

The discrete set of expansion coefficients C_m completely determines I.

Next, one substitutes equations (28) into equation (26) and obtains

13

$$\frac{\partial}{\partial z} \sum_{n=1}^{\infty} W_n(s) A_n(s) \sin p_n z - \gamma^2 \sum_{n=0}^{\infty} W_n(s) B_n(s) \cos p_n z$$

$$= - s \epsilon_0 \overline{E}_z^{inc}(z,s) \tag{33}$$

where

$$A_n(s) = \int_b^{L+b} dz' \sin p_n z' \frac{\partial}{\partial z'} I(z',s) \tag{34}$$

and

$$B_n(s) = \int_b^{L+b} dz' \cos p_n z' I(z',s) \tag{35}$$

Performing an integration by parts in equation (34) and making use of equation (30), one finds that A_n and B_n are related:

$$A_n(s) = - p_n B_n(s) \tag{36}$$

Substituting equation (32) into equation (35), one has

$$B_n(s) = \sum_{m=1}^{\infty} \alpha_{nm} C_m(s) \tag{37}$$

where

$$\alpha_{nm} = \int_b^{L+b} dz' \cos p_n z' \sin k_m(z' - b) \tag{38}$$

Note that the index n runs from 0 to ∞ while the index m runs from 1 to ∞ .

Equation (33) can be regarded as a vector relation in the infinite-dimensional vector space. The component of this relation along the basis vector $\sin k_m(z - b)$ can be obtained by multiplying equation (33) by $\sin k_m(z - b)$ and integrating over z from b to $L+b$. The derivative in the first term is again treated by integration by parts. The result then is

$$\sum_{n=1}^{\infty} \beta_{nm} k_m W_n(s) A_n(s) + \gamma^2 \sum_{n=0}^{\infty} \alpha_{nm} W_n(s) B_n(s) = D_m(s) \tag{39}$$

14

where

$$\beta_{nm} = \int_b^{L+b} dz \, \sin p_n z \, \cos k_m (z-b) \tag{40}$$

and

$$D_m(s) = s\epsilon_o \int_b^{L+b} dz \, \sin k_m (z-b) \overline{E}_z^{inc}(z,s) \tag{41}$$

It is not difficult to see that α_{nm} and β_{nm} are related:

$$\beta_{nm} k_m = -p_n \alpha_{nm} \tag{42}$$

Substituting equations (36), (37) and (42) into equation (39), one obtains a matrix equation for the expansion coefficients C_ℓ:

$$\sum_{\ell=1}^{\infty} M_{m\ell}(s) C_\ell(s) = D_m(s) \tag{43}$$

where

$$M_{m\ell}(s) = \sum_{n=0}^{\infty} (\gamma^2 + p_n^2) W_n(s) \alpha_{nm} \alpha_{n\ell} \tag{44}$$

The matrix M is symmetric $(M_{m\ell} = M_{\ell m})$ but not Hermitian $(M_{m\ell} \neq M_{\ell m}^*)$.

SECTION V

APPROXIMATE ANALYTICAL SOLUTION

The matrix equation (43) is a concise and exact formulation of the simulator/test-object interaction problem. From the standpoint of solving the problem it is also a convenient starting point. For example, an accurate numerical solution can always be obtained by using standard methods in numerical matrix calculus. In the following, however, an approximate analytical solution will be constructed instead.

The approximation employed below is based on the observation that the diagonal elements of the matrix M in equation (43) are considerably greater than the off-diagonal elements. The reason behind this disparity is as follows. If one examines closely the structure of the matrix element $M_{m\ell}$ given in equation (44), one finds that the combination $\alpha_{nm}\alpha_{n\ell}$ has the most violent variation with the summation index n . It has therefore a great effect on the value of $M_{m\ell}$. The factor α_{nm} can be evaluated from equation (38):

$$\alpha_{nm} = \frac{k_m}{k_m^2 - p_n^2}\left[\cos p_n b - (-1)^m \cos p_n (L+b)\right] \qquad (45)$$

It assumes both positive and negative values. In an off-diagonal matrix element $M_{m\ell}$ with $m \neq \ell$, these positive and negative values of α_{nm} and $\alpha_{n\ell}$ to a considerable extent mutually cancel out during the summation over n . However, the situation is different with a diagonal matrix element M_{mm} . With $m = \ell$, the product $\alpha_{nm}\alpha_{n\ell}$ becomes the square α_{nm}^2 which is always positive. It contributes constructively to M_{mm} , and adds up to a large value. For small values of m and ℓ , sample numerical calculations show that the diagonal elements are one order of magnitude greater than the off-diagonal ones. The disparity is expected to increase for larger values of m and ℓ .

This property of the matrix elements is the basis of an approximation scheme for solving the matrix equation (43). One first rearranges the equation in the form

$$M_{mm}(s)C_m(s) = D_m(s) - \sum_{\substack{\ell=1 \\ \ell \neq m}}^{\infty} M_{m\ell}(s)C_\ell(s) \qquad (46)$$

16

The diagonal element M_{mm} has been taken out from the sum. The remaining sum contains only off-diagonal elements, and is regarded as a perturbation. A first approximation to the solution of equation (46) is therefore

$$C_m^{(1)}(s) = \frac{D_m(s)}{M_{mm}(s)} \qquad (47)$$

Successive approximations can be obtained by iteration. For example, the second approximation is

$$C_m^{(2)}(s) = \frac{D_m(s)}{M_{mm}(s)} - \sum_{\substack{\ell=1 \\ \ell \neq m}}^{\infty} \frac{M_{m\ell}(s)}{M_{mm}(s)} C_\ell^{(1)}(s) \qquad (48)$$

In the following sections the solution in the first approximation will be examined.

SECTION VI

COMPLEX-FREQUENCY-PLANE SINGULARITIES

In the first approximation of equation (47) the total axial current induced on the cylinder is given by

$$I(z,s) = \sum_{m=1}^{\infty} \frac{D_m(s)}{M_{mm}(s)} \sin k_m(z - b) \tag{49}$$

In the time domain this current becomes

$$I(z,t) = \frac{1}{2\pi j} \int_{C-j\infty}^{C+j\infty} ds \; e^{st} \sum_{m=1}^{\infty} \frac{D_m(s)}{M_{mm}(s)} \sin k_m(z - b) \tag{50}$$

where C is an appropriate positive constant. The value of the integral is dependent on the singularities of the integrand in the left half of the complex s-plane. The parameters of these singularities can be used to characterize the excitation of the cylinder.

The s-plane singularities can be grouped into three classes. The first class consists of singularities of the factor D_m. By equation (41) these singularities are introduced by the frequency dependence of the incident electric field E_z^{inc}. The second class consists of singularities of the factor M_{mm}. By equation (44) these singularities are contained in the function W_n defined in equation (29). From the well-known analytical properties of the modified Bessel functions, one concludes that these singularities are branch cuts with branch points determined by the vanishing of the argument of the function $K_o(\sqrt{\gamma^2 + p_n^2}\, a)$. By equation (7) the branch points are located at

$$s = \pm j \frac{n\pi c}{h} \qquad n = 0,1,2,\ldots \tag{51}$$

along the imaginary axis. They are characteristic of the parallel-plate waveguide, and depend neither on the length L nor the radius a of the cylinder. In fact they correspond to the excitation thresholds of the waveguide propagation modes. Examples of these waveguide mode singularities are shown in figure 2.

18

Im $\frac{sh}{\pi c}$
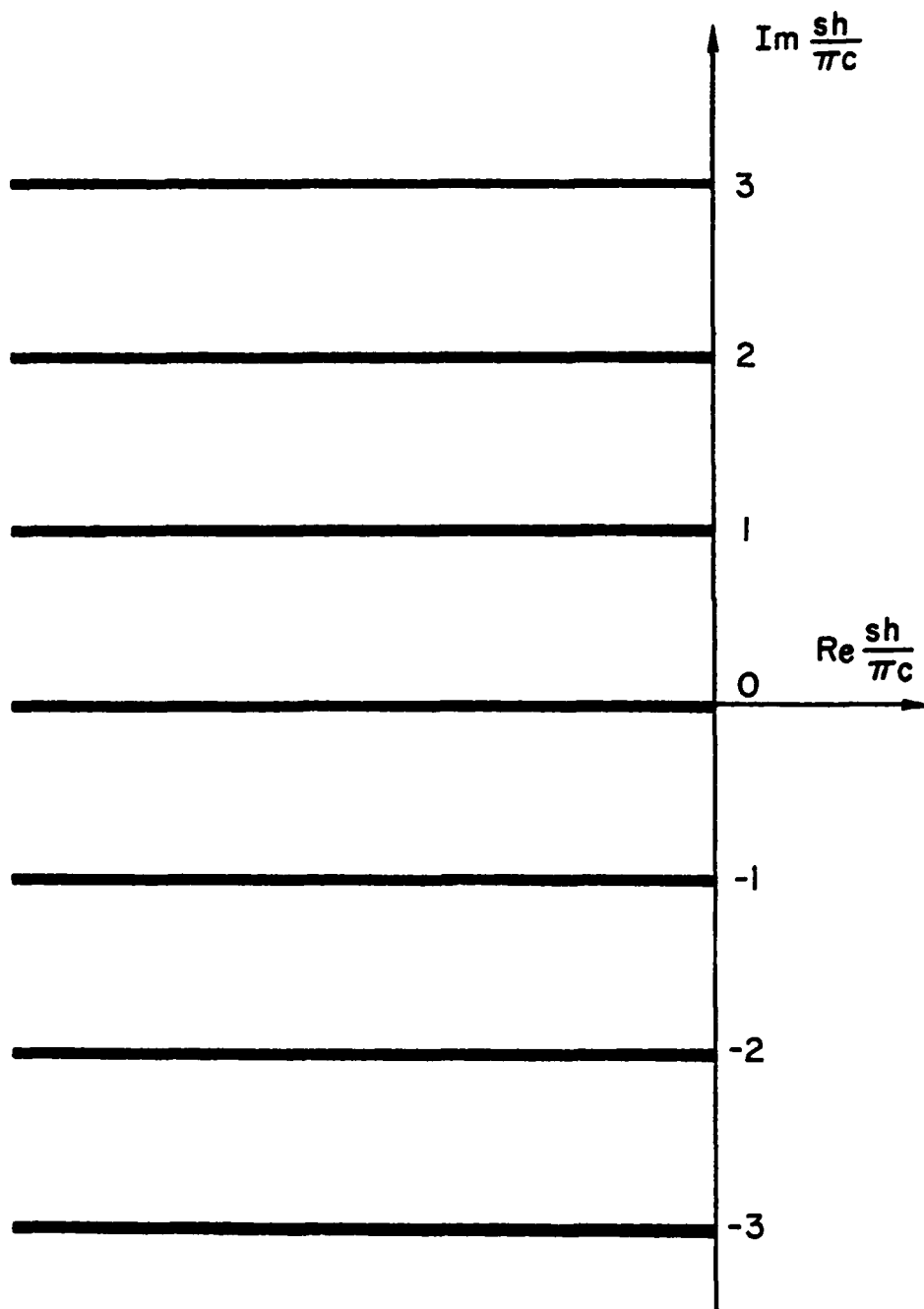
Re $\frac{sh}{\pi c}$

3

2

1

0

-1

-2

-3

Figure 2. Branch-Cut Singularities in the Complex-Frequency Plane
Characterizing the Waveguide Modes

The third class of s-plane singularities consists of the zeros of M_{mm}. They give rise to poles in the integrand of equation (50), and are determined by solving the transcendental equation

$$M_{mm}(s) = \sum_{n=0}^{\infty} \left(\frac{s^2}{c^2} + p_n^2 \right) W_n(s) \alpha_{nm}^2 = 0 \qquad m = 1,2,3,\ldots \qquad (52)$$

The solutions depend on all the parameters h, L and a of the model. They can be interpreted as the natural frequencies of certain natural modes of the surface current on the cylinder. For each m, there are two solutions of equation (52) which form a complex-conjugate pair. They lie in the second and third quadrants of the s-plane. The natural modes corresponding to these natural frequencies are the sine functions in equation (50). Thus, in this approximation, the natural modes are simple sinusoidal currents.

Let the solution of equation (52) in the second quadrant be denoted by s_m. The other solution is its complex conjugate s_m^* in the third quadrant. Decompose s_m into its real and imaginary parts:

$$s_m = s_m' + j s_m'' \qquad (53)$$

In principle, s_m' and s_m'' can be obtained accurately by numerical techniques. In the following, however, one will be content with deriving approximate analytical expressions. The method of approximation will be based on the assumption that the two poles lie close to the imaginary axis, so that they can be approximately located by observing their influence on the behavior of M_{mm} along the imaginary axis.

On the imaginary s-axis, let

$$s = j\omega, \qquad \gamma = jk \qquad (54)$$

where ω and k are both real and vary from $-\infty$ to ∞. They are related by

$$\omega = kc \qquad (55)$$

The function W_n can be decomposed into its real and imaginary parts:

$$W_n(j\omega) = W'_n(\omega) + j W''_n(\omega) \tag{56}$$

By equations (15) and (29), one has

$$W'_n(\omega) = \frac{1}{\pi h \epsilon_n} I_0\left(\sqrt{p_n^2 - k^2}\, a\right) K_0\left(\sqrt{p_n^2 - k^2}\, a\right) \theta\left(p_n^2 - k^2\right)$$

$$- \frac{1}{2h\epsilon_n} J_0\left(\sqrt{k^2 - p_n^2}\, a\right) Y_0\left(\sqrt{k^2 - p_n^2}\, a\right) \theta\left(k^2 - p_n^2\right)$$

$$W''_n(\omega) = - \frac{\omega}{|\omega|} \frac{1}{2h\epsilon_n} J_0^2\left(\sqrt{k^2 - p_n^2}\, a\right) \theta\left(k^2 - p_n^2\right) \tag{57}$$

where J_0 and Y_0 are the Bessel and Neumann functions, and θ is the unit step function:

$$\theta(x) = \begin{cases} 1 & x > 0 \\ \\ 0 & x < 0 \end{cases} \tag{58}$$

The square roots in equation (57) are all considered positive.

In a similar manner the value of M_{mm} along the imaginary axis can be decomposed into its real and imaginary parts:

$$M_{mm}(j\omega) = M'_{mm}(\omega) + j M''_{mm}(\omega) \tag{59}$$

with

$$M'_{mm}(\omega) = \sum_{n=0}^{\infty} \left(- \frac{\omega^2}{c^2} + p_n^2\right) W'_n(\omega) \alpha_{nm}^2$$

$$M''_{mm}(\omega) = \sum_{n=0}^{\infty} \left(- \frac{\omega^2}{c^2} + p_n^2\right) W''_n(\omega) \alpha_{nm}^2 \tag{60}$$

When $j\omega$ is close to the solution s_m of equation (52) in the second quadrant, M'_{mm} can be seen to pass through a zero. This property is used to determine s''_m approximately:

21

$$M'_{mm}(s''_m) = 0 \qquad\qquad (61)$$

which is a transcendental equation involving real quantities only. It is simpler to solve than the original complex equation (52).

A practical technique to solve equation (61) is by iteration. Using equation (60) one can rewrite it as

$$s''_m = c \left[\frac{\sum\limits_{n=0}^{\infty} p_n^2 W'_n(s''_m) \alpha_{nm}^2}{\sum\limits_{n=0}^{\infty} W'_n(s''_m) \alpha_{nm}^2} \right]^{\frac{1}{2}} \qquad\qquad (62)$$

The iteration is performed by successively substituting trial solutions into the right-hand side and deriving improved approximations on the left-hand side. In the appendix it is shown that, in the infinitely thin cylinder limit, the solution of equation (62) is simply

$$s''_m = k_m c = \frac{m\pi c}{L} \qquad \text{for} \quad \frac{a}{L} \to 0 \qquad\qquad (63)$$

Hence, for a thin cylinder, one can use this result to start the iteration. An improved approximation to s''_m is therefore

$$s''_m = c \left[\frac{\sum\limits_{n=0}^{\infty} p_n^2 W'_n(k_m c) \alpha_{nm}^2}{\sum\limits_{n=0}^{\infty} W'_n(k_m c) \alpha_{nm}^2} \right]^{\frac{1}{2}} \qquad\qquad (64)$$

The following calculation will be based on this approximate solution of equation (61).

In the neighborhood of this solution, M'_{mm} has the following approximate expansion:

$$M'_{mm}(\omega) \simeq - \Omega_m(\omega - s''_m) \qquad\qquad (65)$$

where s_m'' is given by equation (64) and Ω_m is a real quantity defined by

$$\Omega_m = \frac{2s_m''}{c^2} \sum_{n=0}^{\infty} W_n'(k_m c) \alpha_{nm}^2 \tag{66}$$

The imaginary part M_{mm}'' has a hump around this solution and can be approximated by its value at $\omega = k_m c$:

$$M_{mm}''(\omega) \simeq M_{mm}''(k_m c) \tag{67}$$

Gathering together these results, one finds that the complex function M_{mm} has the expansion

$$M_{mm}(j\omega) \simeq -\Omega_m(\omega - s_m'' + j s_m') \qquad \text{for} \quad \omega \simeq s_m'' \tag{68}$$

where

$$s_m' = -\frac{1}{\Omega_m} M_{mm}''(k_m c) \tag{69}$$

Equation (68) shows that, in the complex s-plane $(j\omega \to s)$, the function M_{mm} has a zero at $s_m = s_m' + j s_m''$. Therefore the reciprocal of M_{mm} has a pole at the same point. In the neighborhood of this point, one has

$$\frac{1}{M_{mm}(s)} \simeq \frac{-j}{\Omega_m(s - s_m)} \qquad \text{for} \quad s \simeq s_m \tag{70}$$

Similarly, by repeating the calculation in the third quadrant, one finds that M_{mm} has a second zero at s_m^* , and that

$$\frac{1}{M_{mm}(s)} \simeq \frac{j}{\Omega_m(s - s_m^*)} \qquad \text{for} \quad s \simeq s_m^* \tag{71}$$

In summary, the total axial current on the cylinder given in equation (49) has the following expansion in the complex s-plane:

23

$$I(z,s) = \sum_{m=1}^{\infty} \left[\frac{R_m(z)}{s - s_m} + \frac{R_m^*(z)}{s - s_m^*} \right] + \Psi(z,s) \qquad (72)$$

It consists of a sum of simple poles and a remainder term Ψ. For each value of m there is a pair of poles situated at

$$s_m = s_m' + j s_m'' \qquad \text{and} \qquad s_m^* = s_m' - j s_m'' \qquad (73)$$

where s_m' and s_m'' are approximately given by equations (64) and (69). By equations (41), (49) and (70), the residue R_m is

$$R_m(z) = - \frac{j D_m(s_m)}{\Omega_m} \sin k_m(z - b)$$

$$= - \frac{j s_m \epsilon_o}{\Omega_m} \sin k_m(z - b) \int_b^{L+b} dz' \sin k_m(z' - b) \overline{E}_z^{inc}(z', s_m) \qquad (74)$$

These poles correspond to the natural modes of the cylinder. The remainder Ψ contains all other contributions from the branch cuts of the waveguide modes as well as whatever singularities the incident electric field may introduce.

24

SECTION VII

NUMERICAL RESULTS

The three quantities s_m' , s_m'' and Ω_m , characteristic of the simple-pole
singularities in the complex s-plane, are given analytically in equations (64),
(66) and (69). In the following they are evaluated numerically as functions
of the geometrical parameters h , a , L and the natural-mode index m . One
takes a case in which the cylinder is situated midway between the two parallel
plates, so that

$$b = (h - L)/2 \quad \text{and} \quad L + b = (h + L)/2 \tag{75}$$

This is a highly symmetric situation. Accordingly, the quantity α_{nm} assumes
a simple form:

$$\alpha_{nm} = \frac{2k_m}{k_m^2 - p_n^2} \begin{cases} \cos \dfrac{n\pi}{2} \cos \dfrac{p_n L}{2} & m \text{ odd}, \quad n \text{ even} \\[2ex] \sin \dfrac{n\pi}{2} \sin \dfrac{p_n L}{2} & m \text{ even}, \quad n \text{ odd} \\[2ex] 0 & \text{otherwise} \end{cases} \tag{76}$$

Thus α_{nm} is nonzero only if n and m are of opposite parities.

The numerical calculation is performed for the first six natural modes
(m = 1 to 6) . One picks four values of the ratio a/L :

$$\frac{a}{L} = 0.003, \quad 0.01, \quad 0.03, \quad 0.1 \tag{77}$$

and three values of the ratio L/h :

$$\frac{L}{h} = 0.2, \quad 0.5003, \quad 0.8003 \tag{78}$$

The results are shown in tables 1 to 3. They are also plotted in figures 3 to 5.

The odd choices of the last two values of L/h in equation (78) need
immediate explanation. When the ratio L/h is given simple, rational values

Table 1

POLE SINGULARITY PARAMETERS FOR L/h = 0.2

m	$\dfrac{a}{L}$	$\dfrac{s'_m L}{\pi c}$	$\dfrac{s''_m L}{\pi c}$	$2\pi c\Omega_m$
1	0.003	−0.085	0.935	14.5
	0.01	−0.114	0.927	10.9
	0.03	−0.162	0.917	7.59
	0.1	−0.290	0.918	4.09
2	0.003	−0.117	1.91	27.0
	0.01	−0.160	1.91	19.7
	0.03	−0.238	1.91	13.1
	0.1	−0.460	1.98	6.03
3	0.003	−0.138	2.90	38.7
	0.01	−0.192	2.90	27.7
	0.03	−0.293	2.91	17.8
	0.1	−0.578	3.09	7.16
4	0.003	−0.154	3.89	49.8
	0.01	−0.217	3.89	35.2
	0.03	−0.337	3.92	21.9
	0.1	−0.647	4.22	7.86
5	0.003	−0.167	4.88	60.6
	0.01	−0.238	4.89	42.3
	0.03	−0.374	4.94	25.7
	0.1	−0.674	5.33	8.30
6	0.003	−0.179	5.88	71.1
	0.01	−0.257	5.89	49.1
	0.03	−0.406	5.95	29.1
	0.1	−0.671	6.42	8.61

Table 2

POLE SINGULARITY PARAMETERS FOR L/h = 0.5003

m	$\frac{a}{L}$	$\frac{s'_m L}{\pi c}$	$\frac{s''_m L}{\pi c}$	$2\pi c\Omega_m$
1	0.003	−0.052	0.952	19.1
	0.01	−0.064	0.950	15.5
	0.03	−0.081	0.950	12.2
	0.1	−0.109	0.963	8.73
2	0.003	−0.126	1.94	26.7
	0.01	−0.174	1.93	19.2
	0.03	−0.266	1.91	12.5
	0.1	−0.557	1.99	5.35
3	0.003	−0.094	2.90	49.3
	0.01	−0.119	2.91	38.6
	0.03	−0.155	2.93	28.9
	0.1	−0.186	3.03	18.4
4	0.003	−0.165	3.93	49.1
	0.01	−0.236	3.92	34.1
	0.03	−0.379	3.93	20.6
	0.1	−0.848	4.27	6.47
5	0.003	−0.117	4.88	76.4
	0.01	−0.152	4.90	58.6
	0.03	−0.199	4.95	42.3
	0.1	−0.176	5.10	25.1
6	0.003	−0.191	5.92	69.8
	0.01	−0.280	5.92	47.4
	0.03	−0.458	5.97	27.1
	0.1	−0.976	6.61	6.54

Table 3

POLE SINGULARITY PARAMETERS FOR $L/h = 0.8003$

| m	$\dfrac{a}{L}$	$\dfrac{s'_m L}{\pi c}$	$\dfrac{s''_m L}{\pi c}$	$2\pi c\Omega_m$
1	0.003	−0.114	0.956	14.1
	0.01	−0.154	0.947	10.4
	0.03	−0.226	0.936	7.04
	0.1	−0.431	0.952	3.53
2	0.003	−0.128	1.97	26.9
	0.01	−0.177	1.97	19.5
	0.03	−0.266	1.99	12.8
	0.1	−0.504	2.15	5.77
3	0.003	−0.110	2.97	41.1
	0.01	−0.151	2.98	30.0
	0.03	−0.220	3.01	20.0
	0.1	−0.327	3.21	9.50
4	0.003	−0.061	3.95	77.9
	0.01	−0.075	3.96	63.1
	0.03	−0.090	3.98	49.6
	0.1	−0.065	4.04	35.3
5	0.003	−0.129	4.88	64.6
	0.01	−0.180	4.87	46.1
	0.03	−0.270	4.88	29.2
	0.1	−0.447	5.02	10.6
6	0.003	−0.182	5.86	70.2
	0.01	−0.265	5.85	48.0
	0.03	−0.435	5.86	27.7
	0.1	−1.25	6.22	5.76
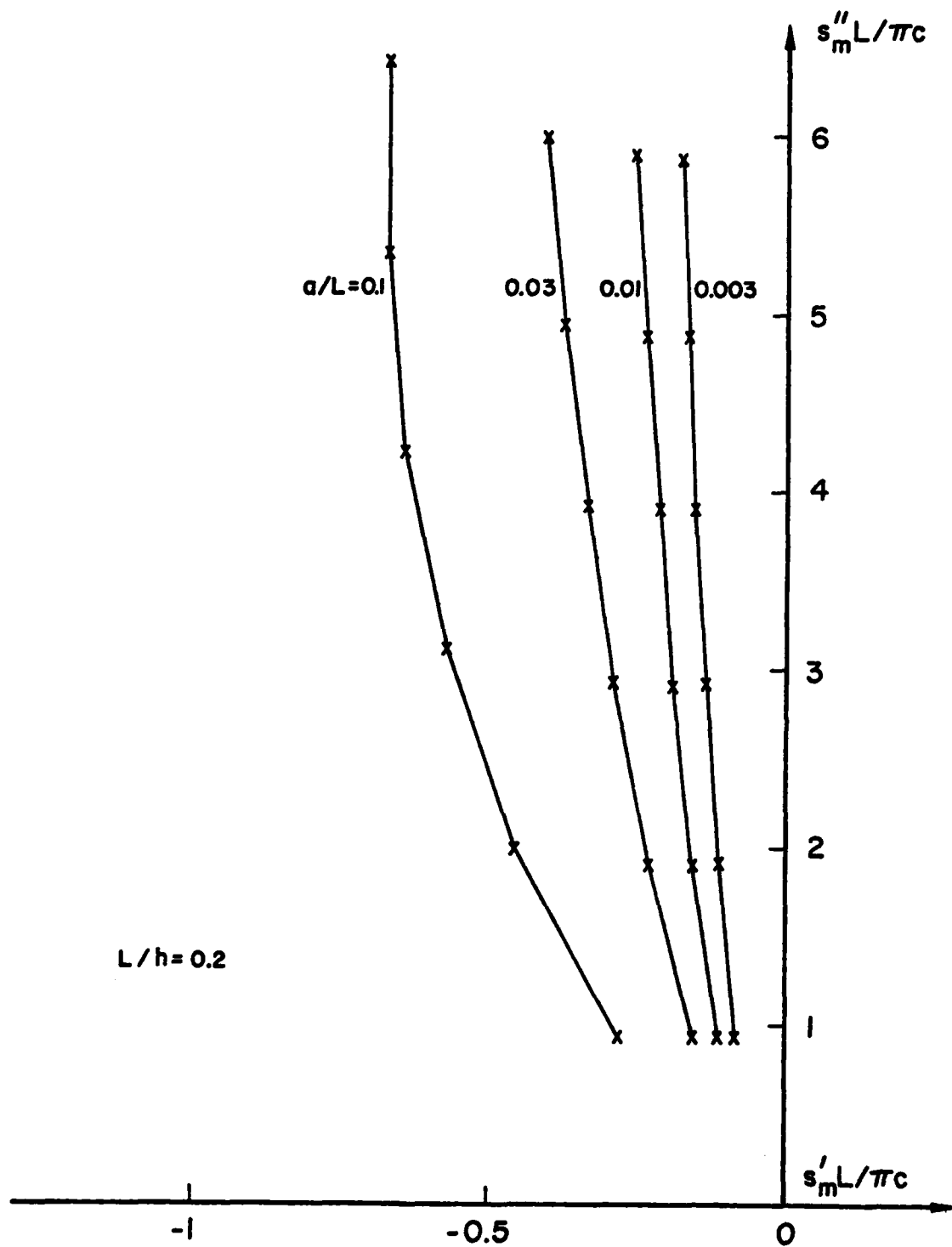
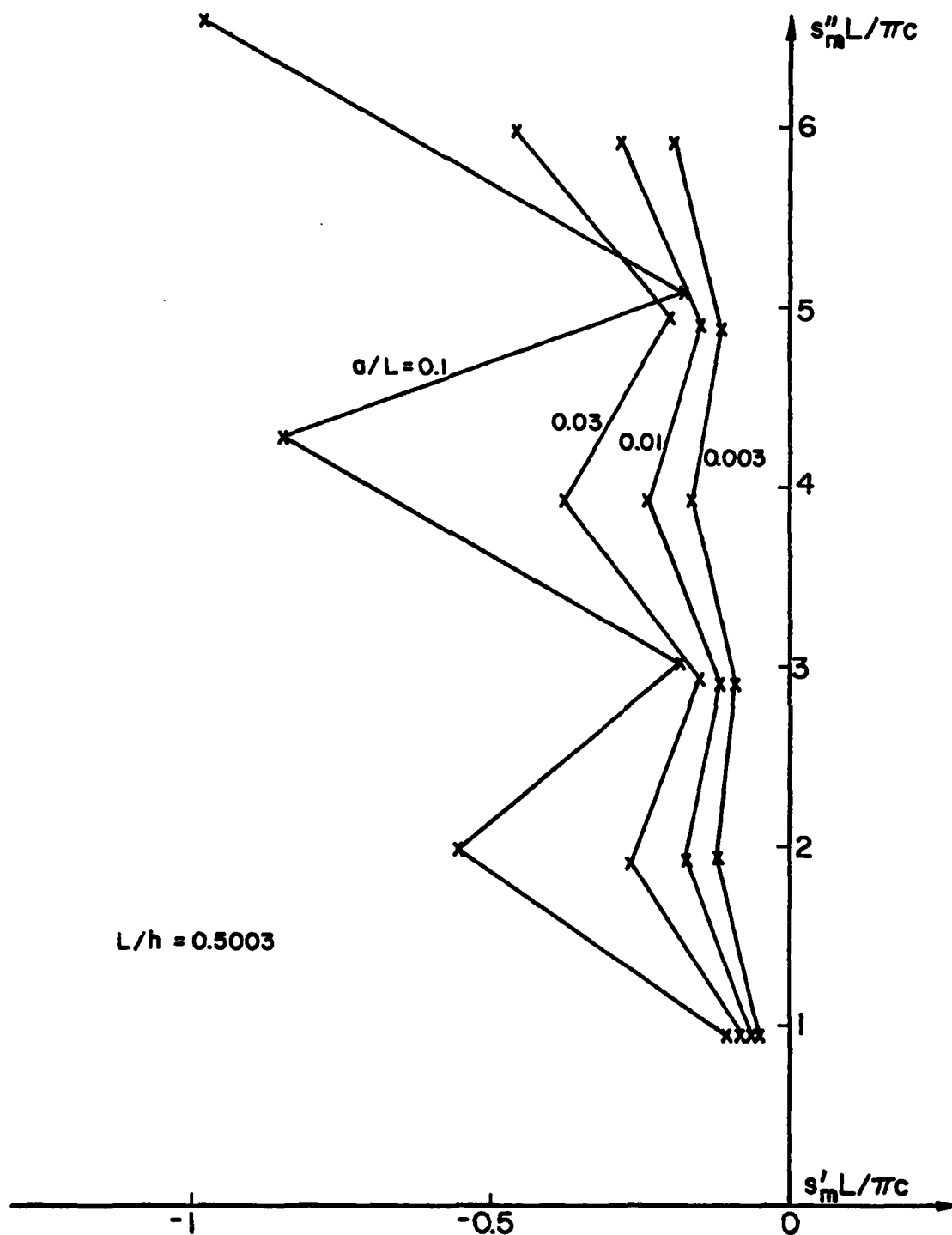Figure 3. Pole Singularities in the Complex-Frequency Plane for L/h = 0.2

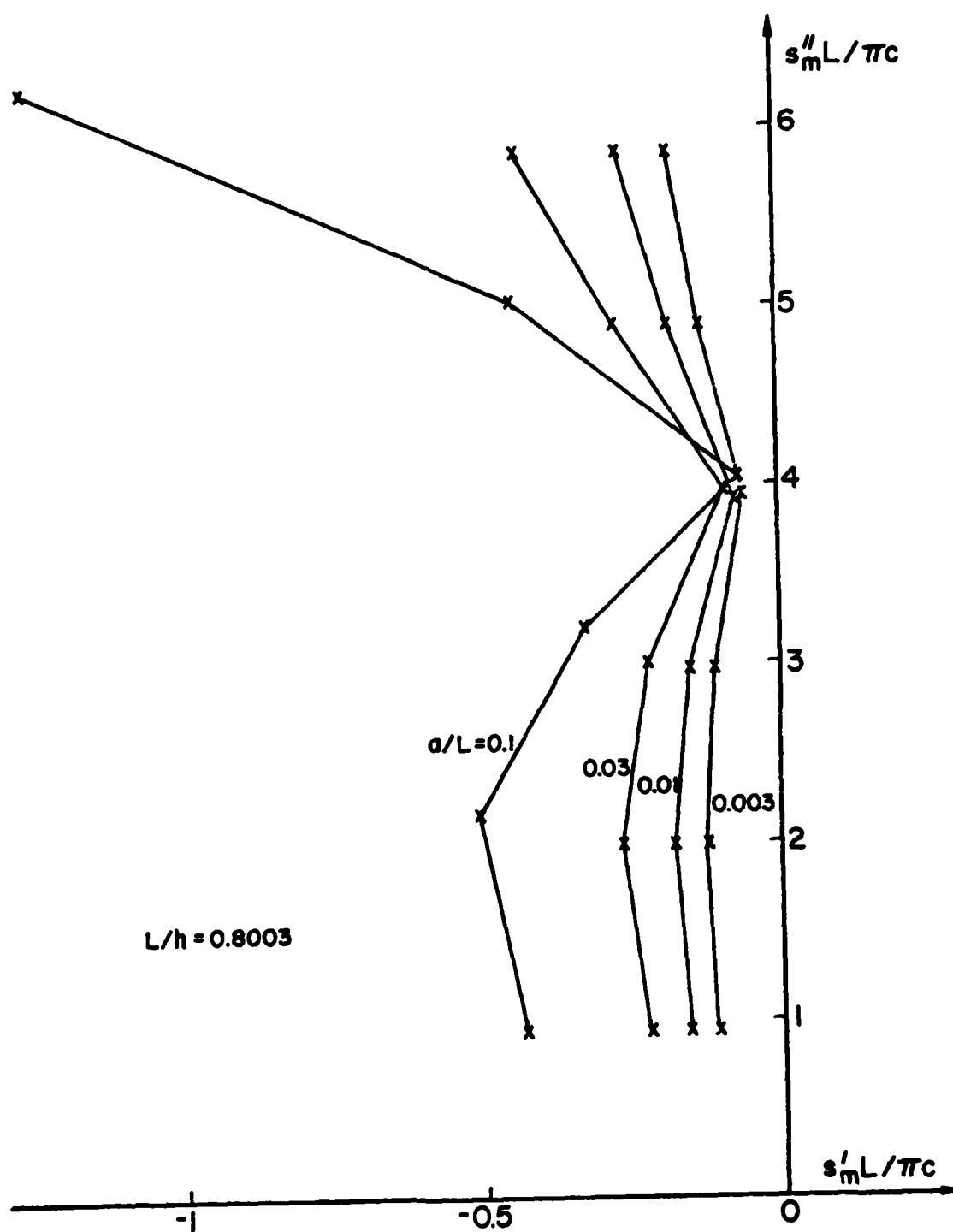Figure 4. Pole Singularities in the Complex-Frequency Plane for L/h = 0.5003

Figure 5. Pole Singularities in the Complex-Frequency Plane for L/h = 0.8003

such as 0.5, it may happen that, for a certain pair of integers m and n, the following equality holds:

$$k_m = p_n \tag{79}$$

In this event one finds a logarithmic divergence in equation (64) arising from the exact vanishing of the argument of the function K_o or Y_o. This divergence nevertheless is not really there, and can be traced back to a harmless term vanishing as $\epsilon \, \ell n \, \epsilon$ in the function M_{mm}. It is introduced into the picture through the iterative scheme of equation (62) and the use of $k_m c$ as the first trial solution in equation (64). It can be easily avoided by starting the iteration with a slightly different trial solution. An alternative procedure is to alter the ratio L/h by a small amount. For example, the ratio $L/h = 0.5$ can be replaced by $L/h = 0.5003$, thereby destroying the equality (79).

For $m = 1$ to 6 and n of opposite parity to m, the equality is not satisfied for $L/h = 0.2$. However, for $L/h = 0.5$, equation (79) holds for $m = 1$, 3 and 5. For $L/h = 0.8$, it holds for $m = 4$. Accordingly, in the numerical calculation, the last two simple values of L/h are changed slightly to 0.5003 and 0.8003.

Even though no divergence really occurs, equation (79) still clearly represents a condition of resonance and should lead to observable effects. The resonance results from the equality of the wavelengths of certain characteristic excitations on the cylinder and in the waveguide. Its effects are quite evident in figures 3 to 5. At precisely those values of m enumerated in the preceding paragraph, the complex poles show a decided shift toward the imaginary axis. This means that the corresponding natural modes of the cylinder are only weakly damped. Thus, under the excitation of a broadband incident wave, the response of the cylinder will be predominantly in these special modes.

All the results in tables 1 to 3 are of course obtained by using the first-iterated solution of equation (62). The quality of this solution can

be measured by comparing the output value of s_m'' with its input trial value $k_m c$. The tables show that these two values are very close. Specifically, the calculated value of $s_m'' L/\pi c$ is very close to m . This agreement can be taken as an indication of the reliability of the first-iterated solution.

SECTION VIII

CONCLUSIONS

It is possible to draw a number of general conclusions from the specific numerical results.

The effects of the simulator/test-object interaction are clearly seen in figures 3 to 5. The locations of the poles in the complex-frequency plane, corresponding to the natural modes of the current on the cylinder, are strongly dependent on the length-to-separation ratio L/h . When L/h is small, the dimensions of the simulator are much greater than those of the test object. The simulator/test-object interaction is weak, at least for the lowest few natural modes. For example, the distribution of the poles in figure 3 for $L/h = 0.2$ is not substantially different from that in the case of a thin cylinder in free space (ref. 3). As the ratio L/h is increased, the effects of the interaction strengthen; the poles are shifted violently around. The dependence of their movement on L/h , however, is not monotonic but rather oscillatory and in the nature of resonances. For a given ratio L/h, modes that satisfy the resonance condition (79) are heavily favored by the simulator/ test-object interaction, in the sense that they are only weakly damped. These resonant cases are exemplified by the numerical results in figures 4 and 5.

The poles, however, are not sufficient in themselves to provide a complete measure of the simulator/test-object interaction. The presence of the simulator structure indroduces additional singularities into the complex-frequency plane. For the parallel-plate bounded-wave simulator in this problem, these singularities consist of an infinite number of branch cuts. The contribution from the branch cuts must be considered if one is to obtain a full characterization of the simulator/test-object interaction.

The numerical results of this study are based on an approximate, analytical formula for the solution of an exact matrix equation. It will be worthwhile to attempt an accurate, numerical solution of the matrix equation directly. Such a solution is feasible with the availability of large, advanced computers. It will not only provide accurate technical data, but will also represent a valuable standard whereby the reliability of future analytical investigations can be gauged.

34

REFERENCES

[1] Baum, C.E., "Impedances and Field Distributions for Parallel-Plate
Transmission-Line Simulators," Sensor and Simulation Notes, Note 21,
Air Force Weapons Laboratory, Kirtland Air Force Base, NM, 1966.

[2] Magnus, W. and F. Oberhettinger, Formulas and Theorems for the Functions
of Mathematical Physics, Chelsea, New York (1949), p.21.

[3] Marin, L., "Natural Modes of Certain Thin-Wire Structures," Interaction
Notes, Note 186, Air Force Weapons Laboratory, Kirtland Air Force Base,
NM, 1974.

APPENDIX

THIN-CYLINDER LIMIT

In the thin-cylinder limit $(a/L \to 0)$ equation (62) can be shown to have the simple solution $s_m'' = \pm k_m c$.

By equation (45) the quantity α_{nm}^2 varies like n^{-4} for large n . Thus the contribution to the two sums in equation (62) comes mainly from terms of small n . Because of this property, one can replace the function W_n' by its thin-cylinder limit at small n . By equation (57) one has

$$W_n'(\omega) \to - \frac{1}{\pi h \epsilon_n} \ln\left(\frac{a}{L}\right) \qquad \text{as} \quad \frac{a}{L} \to 0 \tag{A1}$$

Therefore equation (62) becomes

$$\left(\frac{s_m''}{c}\right)^2 = \frac{\sum\limits_{n=0}^{\infty} \frac{1}{\epsilon_n} p_n^2 \alpha_{nm}^2}{\sum\limits_{n=0}^{\infty} \frac{1}{\epsilon_n} \alpha_{nm}^2} \tag{A2}$$

By equation (42) it can also be rewritten as

$$\left(\frac{s_m''}{c}\right)^2 = k_m^2 \frac{\sum\limits_{n=0}^{\infty} \frac{1}{\epsilon_n} \beta_{nm}^2}{\sum\limits_{n=0}^{\infty} \frac{1}{\epsilon_n} \alpha_{nm}^2} \tag{A3}$$

The two sums can be evaluated by invoking equations (38) and (40):

$$\sum\limits_{n=0}^{\infty} \frac{1}{\epsilon_n} \beta_{nm}^2 = \int_b^{L+b} dz \int_b^{L+b} dz' \cos k_m(z-b)\cos k_m(z'-b) \sum\limits_{n=0}^{\infty} \frac{1}{\epsilon_n} \sin p_n z \sin p_n z'$$

$$= \frac{1}{4} Lh$$

37

$$\sum_{n=0}^{\infty} \frac{1}{\epsilon_n} \alpha_{nm}^2 = \int_b^{L+b} dz \int_b^{L+b} dz' \sin k_m(z-b) \sin k_m(z'-b) \sum_{n=0}^{\infty} \frac{1}{\epsilon_n} \cos p_n z \cos p_n z'$$

$$= \frac{1}{4} Lh \tag{A4}$$

where use has been made of the identities

$$\sum_{n=0}^{\infty} \frac{1}{\epsilon_n} \sin p_n z \sin p_n z' = \frac{h}{2} \delta(z-z')$$

$$\tag{A5}$$

$$\sum_{n=0}^{\infty} \frac{1}{\epsilon_n} \cos p_n z \cos p_n z' = \frac{h}{2} \delta(z-z')$$

for $b < z, z' < L+b$. Substituting equations (A4) into equation (A3) one obtains the simple result

$$s_m'' = \pm k_m c \tag{A6}$$